

Online Tracking of Local Damping in Power Systems with High Proportion of Renewable Energy Sources Under Ambient Data

Zhenglong Sun, Zewei Li, Hao Yang, Lixin Wang, Bo Wang, Chao Pan, Cheng Liu, and Guowei Cai

Abstract—As the proportion of renewable energy sources continues to increase, the local damping contributions of sources in power system decrease, posing a challenge to the power system stability. Therefore, online tracking of the damping contributions of each source is crucial for the prevention of low-frequency oscillations. This paper proposes an online tracking method of local damping under ambient data. The proposed method is based on dissipation energy spectrum analysis (DESA) and the energy dissipation factor (EDF). First, the feasibility of using frequency-domain analysis for the dissipation energy of generator is analyzed. The frequency spectral function of dissipation energy of generator is then derived by integrating with Parseval's theorem, and the EDF is defined. Second, the generator energy dissipation factor (GEDF) for the dominant oscillation mode frequency is established. The modal information of the dominant oscillation in the power system is obtained through DESA. The relationship between the frequency spectral function and eigenvalues is also established. Finally, an online tracking method of local damping is proposed based on DESA and GEDF. The effectiveness of the proposed method is validated through simulations on a four-machine 11-bus power system and an actual power system in Northwest China.

Index Terms—Low-frequency oscillation, renewable energy sources, generator energy dissipation factor (GEDF), dissipation energy spectrum analysis (DESA), local damping, online tracking, frequency domain, energy dissipation factor.

I. INTRODUCTION

THE utilization of wind, solar, and other renewable energy sources in power systems is increasing [1], [2]. This shift is accompanied by the emergence of features characterized by low inertia and damping. Consequently, power systems are becoming more vulnerable to low-frequency oscillations [3]-[5], which could compromise the secure operation.

Damping is a crucial aspect in the study of oscillations. Sources with positive damping dissipate energy during oscillations, thereby aiding the attenuation of oscillations. By contrast, sources with negative damping emit energy during oscillations, thereby exacerbating the oscillations. Alterations in the structural configuration of the power system can cause some sources to exhibit negative damping, which triggers oscillations [6]-[8]. Thus, the online tracking and assessment of local damping and identification of sources with negative damping are crucial for curtailing oscillations and enhancing the power system stability.

The eigenvalue analysis is a classic method in small-disturbance stability analysis [9], [10]. The eigenvalue analysis can be employed to select critical sources and install them in power system stabilizers in multi-machine systems [11]. In addition, this method can be used to assess the stability of electronic-based power systems [12]. The dimensionality increases as the power system scale expands, leading to the curse of dimensionality during the computation of eigenvalues. The curse of dimensionality poses challenges for efficient online analysis. The component of the generator electromagnetic torque, known as damping torque, is an essential factor in studying the dynamic stability of power systems [13]. The principle of weakened system damping in weakly interconnected systems caused by reduced line impedance can be explained using the damping torque method [14]. An analysis of the effects of different generator rotor damping structures on the damping torque coefficients can provide a theoretical foundation for enhancing the power system stability by altering the damping structures [15]. However, the damping torque of generators in multi-machine systems is highly complex, and the online computation of torque coefficients is challenging.

With the implementation of wide-area measurement systems (WAMSs) in power systems, the obtained phasor measurement data play an essential role in real-time state detection [16], [17]. In addition, phasor measurement data support power system stability analysis. A calculation method for network energy flow based on WAMS data is proposed in [18] to address the challenge to constructing an energy function within a system. This method operates independently of the energy function and facilitates energy flow computation using the phasor measurement data. The correlation between the energy consumption of generator and its damping torque

Manuscript received: February 16, 2024; revised: May 7, 2024; accepted: August 5, 2024. Date of CrossCheck: August 5, 2024. Date of online publication: August 26, 2024.

This work was supported by National Key Research and Development Program of China (No. 2021YFB2400800).

This article is distributed under the terms of the Creative Commons Attribution 4.0 International License (<http://creativecommons.org/licenses/by/4.0/>).

Z. Sun (corresponding author), Z. Li, H. Yang, L. Wang, B. Wang, C. Pan, C. Liu, and G. Cai are with the Key Laboratory of Modern Power System Simulation and Control & Renewable Energy Technology, Ministry of Education, Northeast Electric Power University, Jilin, China (e-mail: nedusunzl@neepu.edu.cn; 13179255362@163.com; hao_yang@neepu.edu.cn; wanglxnedu@163.com; dbdlwb@126.com; 31563018@qq.com; 05dylc@163.com; caigw@neepu.edu.cn). DOI: 10.35833/MPCE.2024.000169



in a single-machine infinite-bus system is explored in [19], highlighting the close relationship between system damping and energy dissipation. Furthermore, the energy flow analysis method, which involves signal reconstruction and decomposition, can be employed to investigate low-frequency oscillations in power systems. The consistency between the energy flow and modal analysis methods in multi-system scenarios is demonstrated through derivation in [20]. Finally, [21] derives the damping torque coefficient of multi-machine power systems, defines the energy attenuation coefficient, and rigorously establishes the essential equivalence between the damping torque and energy flow analysis methods.

As the energy flow analysis method aligns with system damping, an online assessment of damping can be achieved using this method [22]. By integrating the energy flow theory with the damping representation in elasticity, an online assessment of local damping during oscillation becomes feasible. Reference [23] proposes a method for identifying oscillation sources by analyzing the energy sources and flows within the network. In [24], the dissipation energy curve is computed using eigenvectors, and the energy dissipation factor (EDF) is defined. Reference [25] separates the average dissipation power across the oscillation modes of varying frequencies. It employs eigenvectors to calculate the energy dissipation coefficient specific to a single mode of generator. In addition, [26] introduces an energy-based method that utilizes phasor measurement data to trace poorly damped natural and forced oscillation sources in power systems. However, the assessment of local damping requires filtering the phasor measurement data. Bandwidth selection significantly affects the evaluation results, and real-time applications are hindered by the substantial amount of data required for assessment.

To overcome the limitations of previous research works, this paper integrates Parseval's theorem with dissipation energy, derives the expression of dissipation energy in frequency domain, and defines a spectral function. The relationship between the spectral function and the eigenvalue is elucidated. Then, through spectral and phase analysis of the derived spectral function, an online tracking method of local damping under ambient data is proposed.

The contributions of this paper are as follows.

1) Based on Parseval's theorem, the frequency spectral function and expression of dissipation energy in frequency domain are derived. An EDF is established based on the modal coupling.

2) The generator energy dissipation factor (GEDF) is defined by analyzing and calculating the amplitude and phase of the spectral function of dissipation energy. The relationship between the spectral function and eigenvalues is analyzed.

3) An online tracking method of local damping in frequency domain under ambient data is proposed, where simulation results verify the effectiveness of the proposed method.

The remainder of this paper is organized as follows. Section II describes the expression of dissipation energy in the frequency domain. Section III introduces the assessment of local damping in frequency domain using EDF. Section IV

introduces the assessment of local damping in frequency domain under ambient data. Section V validates the proposed method through case studies. Section VI concludes this paper.

II. EXPRESSION OF DISSIPATION ENERGY IN FREQUENCY DOMAIN

The feasibility of assessing system damping in the frequency domain can be illustrated through the ambient response of power systems, dissipation energy, and time-frequency transformations of signals.

A. Ambient Response of Power Systems

The differential algebraic equations of a power system can be expressed as:

$$\begin{cases} \dot{\mathbf{x}} = \mathbf{f}(\mathbf{x}, \mathbf{y}) \\ \mathbf{0} = \mathbf{g}(\mathbf{x}, \mathbf{y}, \mathbf{l}) \end{cases} \quad (1)$$

where \mathbf{x} is the state variable of the system; \mathbf{y} is the algebraic variable; \mathbf{l} is the load fluctuation variable; and $\mathbf{f}(\cdot)$ and $\mathbf{g}(\cdot)$ are the continuous functions.

Based on the assumption that the load fluctuations follow an Ornstein-Uhlenbeck distribution, the dynamic model of the load can be expressed as:

$$\dot{\mathbf{l}} = -\mathbf{K}(\mathbf{l} - \mathbf{l}_{eq}) + \delta \boldsymbol{\xi} \quad (2)$$

where \mathbf{l}_{eq} is the load value at the equilibrium point; \mathbf{K} is the load response rate; δ is the noise intensity; and $\boldsymbol{\xi}$ is an ambient fluctuation following a Gaussian distribution.

Linearizing (1) and (2) results in:

$$\begin{bmatrix} \Delta \dot{\mathbf{x}} \\ \Delta \dot{\mathbf{l}} \end{bmatrix} = \begin{bmatrix} \mathbf{f}_x - \mathbf{f}_y \mathbf{g}_y^{-1} \mathbf{g}_x & -\mathbf{f}_y \mathbf{g}_y^{-1} \mathbf{g}_l \\ \mathbf{0} & -\mathbf{K} \end{bmatrix} \begin{bmatrix} \Delta \mathbf{x} \\ \Delta \mathbf{l} \end{bmatrix} + \delta \begin{bmatrix} \mathbf{0} \\ \mathbf{I}_{nl} \end{bmatrix} \boldsymbol{\xi} \quad (3)$$

where \mathbf{g}_x , \mathbf{g}_y , and \mathbf{g}_l are the Jacobian matrices corresponding to variables \mathbf{x} , \mathbf{y} , and \mathbf{l} , respectively; \mathbf{f}_x and \mathbf{f}_y are the Jacobian matrices corresponding to variables \mathbf{x} and \mathbf{y} , respectively; $\Delta \mathbf{x}$ is the change in state variable \mathbf{x} ; $\Delta \mathbf{l}$ is the change in load relative to the equilibrium point; and \mathbf{I}_{nl} is the identity matrix.

$$\text{Let } \mathbf{A} = \begin{bmatrix} \mathbf{f}_x - \mathbf{f}_y \mathbf{g}_y^{-1} \mathbf{g}_x & -\mathbf{f}_y \mathbf{g}_y^{-1} \mathbf{g}_l \\ \mathbf{0} & -\mathbf{K} \end{bmatrix}, \quad \mathbf{z} = \begin{bmatrix} \Delta \mathbf{x} \\ \Delta \mathbf{l} \end{bmatrix}, \quad \text{and } \mathbf{B} = \begin{bmatrix} \mathbf{0} \\ \mathbf{I}_{nl} \end{bmatrix}.$$

Equation (3) can then be represented as:

$$\dot{\mathbf{z}} = \mathbf{A}\mathbf{z} + \delta \mathbf{B}\boldsymbol{\xi} \quad (4)$$

Given that matrix \mathbf{A} contains the characteristic information of electromechanical oscillations under load fluctuations, the eigenvalues $\lambda_k = \sigma_k + j\omega_k$ ($k=1, 2, \dots, n$) corresponding to n electromechanical oscillation modes can be calculated. Therefore, the time-domain analytical solution of the system state variables can be expressed as:

$$\mathbf{z}(t) = \sum_{k=1}^n \mathbf{v}_k \mathbf{u}_k^T \mathbf{z}(0) e^{\sigma_k t} \sin(\omega_k t + \varphi_k) + \delta \mathbf{B}\boldsymbol{\xi} \quad (5)$$

where \mathbf{u}_k and \mathbf{v}_k are the left and right eigenvectors corresponding to eigenvalue λ_k , respectively; $\mathbf{z}(0)$ is the initial value of the state variables; and φ_k is the initial phase of the sinusoidal oscillation for mode k .

The mathematical representation of the ambient response of the power system in (5) consists of two parts: an oscillation component, and a stochastic component that contains

the measurement noise. During normal operation, the power system is subjected to small disturbances uniformly distributed in the spectrum carrying a specific amount of energy. Therefore, when the frequency of environmental excitation is close to that of a specific mode within the power system, oscillation modes are triggered. The following equation (6) shows that the ambient response of the power system contains rich modal information. Let $C_k = \mathbf{v}_k \mathbf{u}_k^T z(0) e^{\sigma_k t}$ and $\varepsilon = \delta \mathbf{B} \zeta$. Substituting these into (5) yields:

$$z(t) = \sum_{k=1}^n C_k \sin(\omega_k t + \varphi_k) + \varepsilon \quad (6)$$

Thus, during the operation of the power system under ambient data, the variations in the active power, reactive power, voltage magnitude, and voltage phase angle at generator port i can be expressed as:

$$\Delta X_i(t) = \sum_{k=1}^n C_{X_i} \sin(\omega_k t + \varphi_{X_i}) + \varepsilon_{noise, X_i} \quad (7)$$

where X_i can be P_i , Q_i , U_i , or θ_i , and P_i , Q_i , U_i , and θ_i are the active power, reactive power, voltage amplitude, and voltage phase angle of generator port i , respectively; and ε_{noise, X_i} is the random component of the measured noise composition in X_i .

B. Theory of Energy Flow

The energy flowing from node i to branch L_{ij} in a power system can be expressed as:

$$W_i = \int \text{Im}(I_{ij}^* dU_i) = \int P_{ij} d\theta_i + \int Q_{ij} d(\ln U_i) \quad (8)$$

where I_{ij} is the current flowing on branch L_{ij} ; P_{ij} and Q_{ij} are the active power and reactive power flowing from node i into branch L_{ij} , respectively; and $\text{Im}(\cdot)$ represents the imaginary part. Here, the term ‘‘energy’’ refers to an energy function derived from Lyapunov functions, which are commonly used to describe the energetic states of systems or objects.

The electrical quantities previously referenced can be presented using steady-state and incremental values as:

$$W_i = W_i^O + W_i^D \quad (9)$$

$$\begin{cases} W_i^O = \int P_{ij,s} d\Delta\theta_i + \int Q_{ij,s} d(\Delta \ln U_i) \\ W_i^D = \int \Delta P_{ij} d\Delta\theta_i + \int \Delta Q_{ij} d(\Delta \ln U_i) = W_i^{D_1} + W_i^{D_2} \end{cases} \quad (10)$$

where Δ is the variation in each electrical quantity; $P_{ij,s}$ and $Q_{ij,s}$ are the steady-state values of active power and reactive power, respectively; W_i^O is the oscillation component representing the transient energy of the power system; W_i^D is the continuously changing component over time, known as the dissipation energy; and $W_i^{D_1}$ and $W_i^{D_2}$ are the integral terms containing the variation in active power and the variation in reactive power, respectively. A positive W_i^D indicates energy consumption that contributes to positive damping, whereas a negative value indicates negative damping. Given the consistency between the dissipation energy and damping torque, the power system damping can be assessed by analyzing the dissipation energy.

The dissipation energy calculated based on the response data from different generator ports includes contributions

from various modal components because the system response to ambient data encompasses multiple modal components. Therefore, the measurement data from generator port i can be used to calculate the dissipation energy W_i^D , and these measurement data enable an analysis of how each mode manifests in dissipating energy. The measurement data from generator port i are substituted into the formula, and the results for $W_i^{D_1}$ and $W_i^{D_2}$ are expressed in (11) and (12), respectively.

$$W_i^{D_1} = \sum_{a=b=1}^n M_a^{P\theta} (t_2 - t_1) + \sum_{a=1, a \neq b=1}^n \sum_{b=1}^n N_{ab}^{P\theta} + \varepsilon_1 \quad (11)$$

$$W_i^{D_2} \approx \sum_{a=b=1}^n M_a^{QU} (t_2 - t_1) + \sum_{a=1, a \neq b=1}^n \sum_{b=1}^n N_{ab}^{QU} + \varepsilon_2 \quad (12)$$

$$W_i^D = W_i^{D_1} + W_i^{D_2} \approx \sum_{a=b=1}^n M_a (t_2 - t_1) + \sum_{a=1}^n \sum_{b=1, a \neq b}^n N_{ab} + \varepsilon_1 + \varepsilon_2 \quad (13)$$

where a and b are the modes; $M_a^{P\theta}$ is the damping term for mode a calculated using the incremental variables $\Delta P_i(t)$ and $\Delta \theta_i(t)$; $N_{ab}^{P\theta}$ is the harmonic and coupling term for modes a and b computed using the incremental variables $\Delta P_i(t)$ and $\Delta \theta_i(t)$; ε_1 is the ambient component in $\Delta P_i(t)$ and $\Delta \theta_i(t)$ composed of measurement noise; M_a^{QU} is the damping term for mode a calculated using the incremental variables $\Delta Q_i(t)$ and $\Delta U_i(t)$; N_{ab}^{QU} is the harmonic and coupling term for modes a and b computed using the incremental variables $\Delta Q_i(t)$ and $\Delta U_i(t)$; ε_2 is the ambient component in $\Delta Q_i(t)$ and $\Delta U_i(t)$ composed of measurement noise, and the derivation is presented in Supplementary Material A; $M_a = M_a^{P\theta} + M_a^{QU}$; and $N_{ab} = N_{ab}^{P\theta} + N_{ab}^{QU}$.

According to (13), between time t_1 and t_2 , the dissipation energy at generator port i is primarily divided into the following three components.

- 1) The first component represents the monotonic damping term that changes over time. This component accumulates contributions from the damping terms of various modes.
- 2) The second component represents the time-varying periodic terms including harmonic terms for different modes and coupling terms between various modes.
- 3) The third component is the ambient term formed by measurement noise.

Time-domain methods ignore the possibility that the frequencies of the harmonic and coupling terms in the second component may match the frequency of the dominant oscillation mode. This oversight can reduce the precision of assessment. Local damping assessment in the frequency domain can solve the aforementioned problem and obtain accurate results. In addition, the sum of the damping terms of the various modes in (13) collectively constitutes the damping of the generator port, indicating the feasibility of assessing local damping in frequency domain.

III. ASSESSMENT OF LOCAL DAMPING IN FREQUENCY DOMAIN USING EDF

Section II presents qualitative analysis of local damping of the power system, which demonstrates the feasibility of

assessing the local damping in frequency domain. The specific generator modes of interest are quantitatively analyzed based on Parseval's theorem. This section presents the expression of dissipation energy under ambient data and introduces the EDF.

A. Parseval's Theorem

Parseval's theorem states that the energy contained in a signal equals the sum of the energies of its components within a complete orthogonal function set. The total energy of a signal in time domain is equal to the total energy of the signal in frequency domain. Here, the term "energy" refers to signal energy, specifically the total energy of signals over a defined period. Use signal $f(t)$ as an example. The following equation is given:

$$\int_{-\infty}^{+\infty} |f(t)|^2 dt = \frac{1}{2\pi} \int_{-\infty}^{+\infty} |F(j\omega)|^2 d\omega \quad (14)$$

where $F(j\omega)$ is obtained from $f(t)$ through Fourier transform.

For two signals $f_i(t)$ and $f_j(t)$, in line with (14), the derivation process is given as:

$$\begin{aligned} \int_{-\infty}^{+\infty} f_i(t)f_j(t)dt &= \int_{-\infty}^{+\infty} f_j(t) \left(\frac{1}{2\pi} \int_{-\infty}^{+\infty} F_i(\omega)e^{j\omega t} d\omega \right) dt = \\ & \frac{1}{2\pi} F_i(\omega) \left(\int_{-\infty}^{+\infty} f_j(t)e^{j\omega t} dt \right) d\omega = \frac{1}{2\pi} \int_{-\infty}^{+\infty} F_i(\omega)F_j^*(\omega) d\omega \end{aligned} \quad (15)$$

where $F_i(\omega)$ and $F_j(\omega)$ are the Fourier transforms of signals $f_i(t)$ and $f_j(t)$, respectively. The integrated product of the two time-domain signals can be transformed into the frequency domain for analysis by applying (15).

B. Local Damping Assessment Index in Frequency Domain Based on Dissipation Energy

Analysis of the generator ports via (10) allows to express the dissipation energy at generator port i as:

$$\begin{aligned} W_{G_i}^D &= \int \Delta P_i(t) d\Delta\theta_i(t) + \int \Delta Q_i(t) d(\Delta \ln U_i(t)) = \\ & \int \Delta P_i(t) \frac{d\Delta\theta_i(t)}{dt} dt + \int \Delta Q_i(t) \frac{d(\Delta \ln U_i(t))}{dt} dt \end{aligned} \quad (16)$$

Let $A(t) = \Delta P_i(t)$, $B(t) = d(\Delta\theta_i(t))/dt$, $C(t) = \Delta Q_i(t)$, and $D(t) = d(\ln U_i(t))/dt$. In this case, the expression for $W_{G_i}^D$ is:

$$W_{G_i}^D = \int A(t)B(t)dt + \int C(t)D(t)dt \quad (17)$$

Fourier transform is then performed on the aforementioned variables. Using $A(t)$ as an example, the transformation process can be expressed as:

$$\begin{aligned} A(j\omega) &= \int_{-\infty}^{+\infty} A(t)e^{-j\omega t} dt = \int_{-\infty}^{+\infty} A(t)\cos(\omega t)dt - \\ & \int_{-\infty}^{+\infty} A(t)j\sin(\omega t)dt = R_A(\omega) - jX_A(\omega) \end{aligned} \quad (18)$$

where $R_A(\omega)$ and $X_A(\omega)$ are the real and imaginary parts of $A(t)$ after Fourier transformation, respectively, and the same applies below.

The results of the Fourier transform reveal that the real and imaginary parts are even and odd functions, respectively, with respect to ω .

Similarly, the remaining variables can be expressed as:

$$\begin{cases} B(j\omega) = R_B(\omega) - jX_B(\omega) \\ C(j\omega) = R_C(\omega) - jX_C(\omega) \\ D(j\omega) = R_D(\omega) - jX_D(\omega) \end{cases} \quad (19)$$

Equations (14), (18), and (19) can be substituted into (17) to obtain:

$$\begin{aligned} W_{G_i}^D &= \int A(t)B(t)dt + \int C(t)D(t)dt = \\ & \frac{1}{2\pi} \left(\int_{-\infty}^{+\infty} A(j\omega)B(j\omega)^* d\omega + \int_{-\infty}^{+\infty} C(j\omega)D(j\omega)^* d\omega \right) \end{aligned} \quad (20)$$

Given that the real parts of the complex numbers obtained from the Fourier transform are all even functions, whereas the imaginary parts are all odd functions, which satisfy the following equations:

$$\begin{cases} \int R_A(\omega)jX_B(\omega)d\omega = 0 \\ \int R_C(\omega)jX_D(\omega)d\omega = 0 \\ \int R_B(\omega)jX_A(\omega)d\omega = 0 \\ \int R_D(\omega)jX_C(\omega)d\omega = 0 \end{cases} \quad (21)$$

The expression of dissipation energy in frequency domain at the generator port can be obtained by substituting (21) into (20) and simplifying the result to obtain:

$$\begin{aligned} W_{G_i}^D &= \int A(t)B(t)dt + \int C(t)D(t)dt = \\ & \frac{1}{2\pi} \int (R_A(\omega)R_B(\omega) + X_A(\omega)X_B(\omega) + \\ & R_C(\omega)R_D(\omega) + X_C(\omega)X_D(\omega))d\omega = \int \zeta(\omega)d\omega \end{aligned} \quad (22)$$

where $\zeta(\omega)$ is the energy spectral function of the dissipation energy. The value of the dissipation energy is equal to the integral of its energy spectral function over the entire frequency domain.

Given that the dissipation energy is composed of the superposition of various modes in the power system, in the analysis of low-frequency oscillation problems, the focus is on the low-frequency modes, particularly the interval oscillation modes that significantly affect the power system stability. Therefore, the dominant oscillation modes must be filtered from the dissipation energy of various modes, and the damping contribution of the source must be assessed. If the frequency of the dissipation energy is divided into multiple frequency intervals with the modal frequency as the center, the dissipation energy at generator port i can be expressed as:

$$\begin{aligned} W_{G_i}^D &= \int \zeta(\omega)d\omega = \int_{\omega_1 - \alpha_{l1}}^{\omega_1 + \alpha_{u1}} \zeta(\omega)d\omega + \\ & \int_{\omega_2 - \alpha_{l2}}^{\omega_2 + \alpha_{u2}} \zeta(\omega)d\omega + \dots + \int_{\omega_k - \alpha_{lk}}^{\omega_k + \alpha_{uk}} \zeta(\omega)d\omega \end{aligned} \quad (23)$$

$$\begin{aligned} W_{G_i}^D &= W_{G_i}^D(f_1) + W_{G_i}^D(f_2) + \dots + W_{G_i}^D(f_k) = \\ & D_{G_i}(f_1) + D_{G_i}(f_2) + \dots + D_{G_i}(f_k) \end{aligned} \quad (24)$$

where ω_k is the angular frequency of the system mode k ; α_{ku} and α_{kl} are the upper and lower limits of the integration interval, respectively, which are used to calculate the dissipation

energy corresponding to mode k ; f_k is the oscillation frequency corresponding to mode k ($\omega_k = 2\pi f_k$); $(f_k - \alpha_{ku}, f_k + \alpha_{kl})$ is the entire integration range of the energy spectral function; and $W_{G_i}^D(f_k)$ is the dissipation energy corresponding to mode k . The integration intervals for the dissipation energy of each mode are connected successively without any overlap. Given that the dissipation energy in the generator is consistent with the damping torque, $D_{G_i}(f_k)$ is defined as the EDF for mode k , which corresponds to generator i . Figure 1 illustrates the division of the theoretical integration intervals corresponding to different modes.

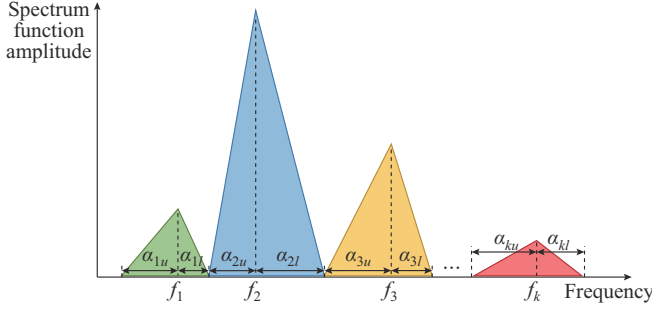


Fig. 1. Division of theoretical integration intervals.

Based on (23), the GEDF is defined as:

$$GD_{G_i}(f_d) = \int_{\omega_d - \beta_d}^{\omega_d + \beta_d} (R_A(\omega)R_B(\omega) + X_A(\omega)X_B(\omega) + R_C(\omega)R_D(\omega) + X_C(\omega)X_D(\omega))d\omega = \int_{\omega_d - \beta_d}^{\omega_d + \beta_d} \zeta(\omega)d\omega \quad (25)$$

where $GD_{G_i}(f_d)$ is the GEDF; and $(\omega_d - \beta_d, \omega_d + \beta_d)$ is the integration interval of the dissipation energy in frequency domain corresponding to the dominant oscillation mode d , and β_d is the optimal integration interval used to calculate the GEDF (generally set to be 0.1 Hz). Although some power systems may have two dominant oscillation modes with similar (distant) frequencies that lead to overlapping (or vacant) parts in the selected integration interval, this phenomenon does not affect the accuracy or effectiveness of the GEDF. Figure 2 shows the selection process of the integration intervals.

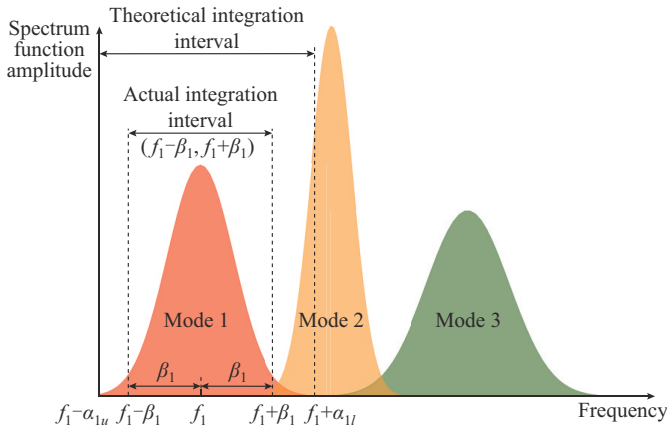


Fig. 2. Selection process of integration intervals.

According to (25), $GD_{G_i}(f_d)$ is the dissipation energy corresponding to mode d . Under dominant oscillation mode d , a large value of $GD_{G_i}(f_d)$ for a source indicates high energy dissipation, which suggests that the source contributes abundant damping to the power system. Positive and negative values of $GD_{G_i}(f_d)$ indicate a positive or negative contribution to the damping, respectively.

C. Relationship Between Spectral Function and Eigenvalues of Dissipation Energy

The time-domain response of a power system under ambient conditions can be represented by the analysis solution given in (5). The relationship between the eigenvalues and energy spectral function is exemplified by using W_i^D . The terms $\Delta P_i(t)$ and $\Delta \theta'_i(t)$ can be expressed as:

$$\Delta P_i(t) = \sum_{k=1}^n v_{pk} u_{pk} P(0) e^{\sigma_k t} \sin(\omega_k t + \varphi_k) + \varepsilon_{noise,P} \quad (26)$$

$$\Delta \theta'_i(t) = \sum_{k=1}^n v_{\theta'k} u_{\theta'k} \theta(0) (\sigma_k e^{\sigma_k t} \sin(\omega_k t + \varphi_k) + \omega_k e^{\sigma_k t} \cos(\omega_k t + \varphi_k)) + \varepsilon_{noise,\theta'} \quad (27)$$

where u_{pk} and v_{pk} are the values of the left and right eigenvectors corresponding to the active power variation for mode k , respectively; and $u_{\theta'k}$ and $v_{\theta'k}$ are the values of the left and right eigenvectors corresponding to the phase angle derivative variation for mode k , respectively.

Performing Fourier transform \mathcal{F} on $\Delta P_i(t)$ yields:

$$\Delta P_i(j\omega) = \mathcal{F} \left(\sum_{k=1}^n v_{pk} u_{pk}^T P(0) e^{\sigma_k t} \sin(\omega_k t + \varphi_k) + \varepsilon_{noise,P} \right) = \sum_{k=1}^n v_{pk} u_{pk}^T P(0) \mathcal{F} \left(e^{\sigma_k t} \frac{e^{j\omega_k t} e^{j\varphi_k} - e^{-j\omega_k t} e^{-j\varphi_k}}{2j} \right) + \varepsilon_P \quad (28)$$

where ε_P is the Fourier transform of the measurement noise in variable $\Delta P_i(t)$.

Given that σ_k represents the real part of the eigenvalue and that only modes with positive damping are considered, the real part of the eigenvalues is negative for $t > 0$ in $\Delta P_i(t)$. Therefore, after the linearity and frequency shift properties of the Fourier transform are leveraged, as shown in (29) and (30), (28) can be transformed into (30).

$$f_P(t) = e^{\sigma_k t} \frac{e^{j\omega_k t} e^{j\varphi_k} - e^{-j\omega_k t} e^{-j\varphi_k}}{2j} \quad (29)$$

$$\mathcal{F}(f_P(t)) = \frac{\omega_k \cos \varphi_k + (\sigma_k + j\omega) \sin \varphi_k}{(\sigma_k + j\omega)^2 + \omega_k^2} \quad (30)$$

$$\Delta P_i(j\omega) = \sum_{k=1}^n v_{pk} u_{pk}^T P(0) \frac{\omega_k \cos \varphi_k + (\sigma_k + j\omega) \sin \varphi_k}{(\sigma_k + j\omega)^2 + \omega_k^2} + \varepsilon_P \quad (31)$$

Similarly, applying Fourier transform to variable $\Delta \theta'_i(t)$ results in:

$$\Delta \theta'_i(j\omega) = \sum_{k=1}^n v_{\theta'k} u_{\theta'k}^T \theta(0) \left[\frac{3\sigma_k \omega_k + 2j\omega \omega_k \cos \varphi_k}{(\sigma_k + j\omega)^2 + \omega_k^2} + \frac{(\sigma_k^2 + j\sigma_k \omega - 2\omega_k^2) \sin \varphi_k}{(\sigma_k + j\omega)^2 + \omega_k^2} \right] + \varepsilon_{\theta'} \quad (32)$$

where $\varepsilon_{\theta'}$ is the Fourier transform of the measurement noise in $\Delta \theta'_i(t)$.

Therefore, when (31) is multiplied by (32), $W_{G_i}^{D_1}$ in (10) can be expressed as:

$$W_{G_i}^{D_1} = \int_{-\infty}^{+\infty} \frac{A(j\omega)B(j\omega)^*}{2\pi} d\omega = \int_{-\infty}^{+\infty} \frac{\Delta P_i(j\omega)\Delta\theta'_i(j\omega)^*}{2\pi} d\omega = \int_{-\infty}^{+\infty} F(\sigma_k, \omega_k, \varphi_k, \omega) d\omega + \varepsilon_{P\theta'} \quad (33)$$

$$F(\sigma_k, \omega_k, \varphi_k, \omega) = \sum_{k=1}^n \mathbf{v}_{pk} \mathbf{u}_{pk}^T \mathbf{v}_{\theta'_k} \mathbf{u}_{\theta'_k}^T P(0)\theta(0) \cdot \left[\frac{\omega_k \cos \varphi_k + (\sigma_k + j\omega) \sin \varphi_k}{2\pi(\sigma_k + j\omega)^2 + \omega_k^2} \left[\frac{3\sigma_k \omega_k + 2j\omega \omega_k \cos \varphi_k}{(\sigma_k + j\omega)^2 + \omega_k^2} + \frac{(\sigma_k^2 + j\sigma_k \omega - 2\omega_k^2) \sin \varphi_k}{(\sigma_k + j\omega)^2 + \omega_k^2} \right]^* \right] \quad (34)$$

where the term obtained by multiplying the measured noise ε_p or $\varepsilon_{\theta'}$ is expressed as $\varepsilon_{P\theta'}$.

Equation (33) indicates that for a system with n oscillation modes, the energy dissipation in the frequency domain can be represented using the real and imaginary parts of the eigenvalues. The relationship between these parameters can be derived via (34).

Similarly, $W_{G_i}^{D_2}$ in (10) can be expressed by function L involving σ_k , ω_k , φ_k , and ω as:

$$W_{G_i}^{D_2} = \frac{1}{2\pi} \int_{-\infty}^{+\infty} C(j\omega)D(j\omega)^* d\omega = \int_{-\infty}^{+\infty} L(\sigma_k, \omega_k, \varphi_k, \omega) d\omega + \varepsilon_{QU} \quad (35)$$

where ε_{QU} is the term multiplied by the noise component.

Accordingly, the dissipation energy in the frequency domain can be represented by (36), which includes the eigenvalue:

$$W_{G_i}^D = \int_{-\infty}^{+\infty} F(\sigma_k, \omega_k, \varphi_k, \omega) + L(\sigma_k, \omega_k, \varphi_k, \omega) d\omega + \varepsilon_{P\theta'} + \varepsilon_{QU} \quad (36)$$

where the original functions $\varepsilon_{P\theta'}$ and ε_{QU} are the noise terms, and their Fourier transforms are obtained by multiplying each element in the vector by the impulse function. In the spectral analysis without considering the fundamental frequency component, $\varepsilon_{P\theta'}$ and ε_{QU} can be disregarded.

Equation (36) can then be rewritten as:

$$W_{G_i}^D = \int (F(\sigma_k, \omega_k, \varphi_k, \omega) + L(\sigma_k, \omega_k, \varphi_k, \omega)) d\omega = \int \xi(\omega) d\omega \quad (37)$$

Equation (37) shows that a certain functional relationship exists between the spectral function of the dissipation energy at the generator port and the real and imaginary parts of the eigenvalues derived from the analysis. The spectral function in each source also contains modal information regarding the power system. This phenomenon indicates that this paper successfully uses the energy spectral function as an indicator and reveals the feasibility of using various online tracking methods to assess the damping in each source.

IV. ASSESSMENT OF LOCAL DAMPING IN FREQUENCY DOMAIN UNDER AMBIENT DATA

A. Identification of Dominant Oscillation Mode Based on Dissipation Energy Spectrum Analysis (DESA)

As the GEDF described in Section III tracks the damping

contribution of each source under ambient data, the dominant oscillation modes of the power system must be identified. In this paper, the modal identification is achieved primarily by applying the DESA method, and the frequency of the dominant oscillation mode and the oscillation area of the power system under that mode can be obtained.

The spectral function of dissipation energy for generator port i can be expressed as:

$$\xi_i(\omega) = R_{\xi_i}(\omega) + jX_{\xi_i}(\omega) = |\xi_i(\omega)| \angle \arctan \frac{X_{\xi_i}(\omega)}{R_{\xi_i}(\omega)} \quad (38)$$

where $R_{\xi_i}(\omega)$ and $X_{\xi_i}(\omega)$ are the real and imaginary parts of the spectral function, respectively. The spectral function can also be presented in terms of the magnitude and phase angle.

First, the amplitude spectrum of the spectral function is analyzed, and then the point with the maximum amplitude in the low-frequency oscillation band is identified. The frequency corresponding to this point (f_d) is the dominant oscillation frequency.

$$|\xi_i(\omega)|_{\max} = |\xi_i(2\pi f_d)| \quad 0.2 \text{ Hz} \leq f_d \leq 2.5 \text{ Hz} \quad (39)$$

Second, the spectral function value of f_d is extracted from $\xi_i(\omega)$ of each generator, and its phase is calculated. Given that the sources participating in the dominant oscillation mode have a phase difference of 180° during the oscillation, the phases of the various sources can be categorized into three types based on their direction and magnitude. The first and second types are the sources with positive and negative phases, respectively, and these sources participate in the dominant oscillation mode. The third type has zero phase, indicating that the sources do not participate in the oscillation.

Identifying the oscillation frequency and area of the dominant oscillation mode could facilitate the development of strategies to enhance the local damping after assessment.

B. Online Tracking of Local Damping

Figure 3 shows a schematic of the online tracking of local damping under ambient data. The main steps of this method are described as follows.

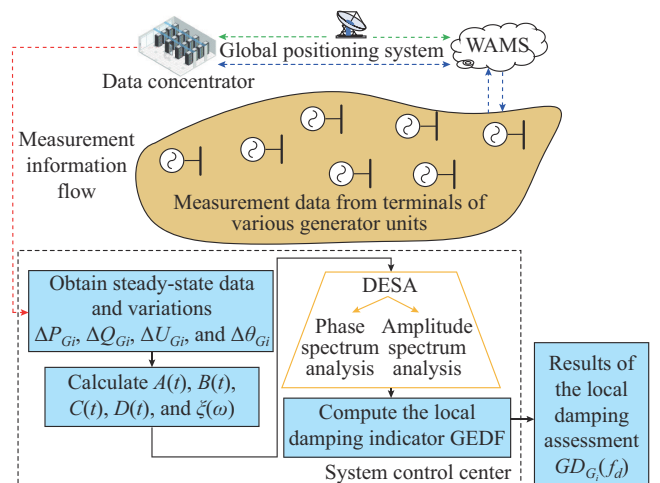


Fig. 3. Online tracking of local damping under ambient data.

Step 1: measurement data are obtained from each generator port under ambient data using a phasor measurement unit. The obtained data include active power, reactive power, voltage magnitude, and voltage phase angle.

Step 2: the response data from *Step 1* are preprocessed, and variations in $\Delta P_i(t)$, $\Delta \theta_i(t)$, $\Delta Q_i(t)$, and $\Delta U_i(t)$ are calculated for the measurement data of each generator port.

Step 3: initial calculations are performed based on the aforementioned variations. The logarithm of the voltage amplitude is obtained, and the derivative of the voltage phase is calculated with respect to time to obtain $A(t)$, $B(t)$, $C(t)$, and $D(t)$. Fourier transform is then conducted on these variables. The energy spectral function $\zeta(\omega)$ is computed, and the DESA method is employed to determine f_d and the partition of generators.

Step 4: based on f_d and the energy spectral function obtained in *Step 3* for each source, a suitable integration interval is used to calculate the local damping assessment index GEDF.

Step 5: the damping contributions of each source are estimated based on the GEDF, and the nature of the contribution is determined by the sign of the GEDF.

C. Discussion

1) Assumptions

Several theoretical assumptions are made in this paper, which may affect the accuracy of local damping assessment. The first assumption is that each source in the power system is equipped with a phasor measurement unit at its generator port, which enables real-time measurements of electrical quantities. The second assumption is that when the local damping is being tracked online, the system operates normally under ambient data. The proposed method is inapplicable to damping assessment during oscillations caused by disturbances in the power system. The third assumption is that during the local damping assessment, the values of some frequency components in the spectral function of the dissipation energy are small and located between two closely spaced modes. It is difficult to precisely determine the modes to which they belong. However, since their effects on the local damping assessment are minimal, they can be ignored.

2) Window Selection

Under simulations conducted in DIGSILENT software, a time step of 0.01 s is used. Accordingly, the sampling interval T_s is 0.01 s, and the sampling frequency of $F_s = 1/T_s = 100$ Hz. The window selection is crucial for assessing the local damping. In power systems, a small window allows for rapid online acquisition of the damping characteristics, thus facilitating timely adjustments to the unstable operating conditions of the power system. However, for an accurate local damping assessment, the minimum frequency spacing d_f of the spectral function is determined by the ratio of the sampling frequency F_s to the window length N . Therefore, a large window results in small d_f , leading to an accurate local damping assessment. Given that the proposed method primarily addresses the low-frequency oscillation modes of the system, a d_f of less than 0.01 Hz is sufficient. Therefore, $d_f = 0.01$ Hz and $N = F_s/d_f = 10000$. In the calculation of GEDF, $\beta_d = 0.1$

Hz, and the integration interval is $(f_d - 0.1 \text{ Hz}, f_d + 0.1 \text{ Hz})$.

3) Advantages

First, when a local damping assessment of the power system is conducted using a spectral function based on the dissipation energy, the coupling between modes is considered. In addition, the integration interval is small, leading to the precise local damping assessment results closely aligned with real-world scenarios. Second, the energy spectral function derived in this paper enables modal partitioning when conducting the local damping assessment. Finally, the proposed method requires minimal data and uses a short window length, making it suitable for online applications.

V. CASE STUDIES

The proposed online tracking method of local damping is validated through simulation using a four-machine 11-bus power system with renewable energy sources and an actual power system in Northwest China. The aim of simulation is to demonstrate the effectiveness of DESA and GEDF.

A. Four-machine 11-bus Power System

Figure 4 illustrates the four-machine 11-bus power system with wind power sources. The original active power output of generator G_2 in this system is 700 MW. In this paper, the active power output of G_2 is adjusted to 100 MW. In addition, a wind farm consisting of 120 wind turbines is connected to bus 6 through a transformer with an active power output of 5 MW for each wind turbine. The dominant oscillation mode of the initial power system is the weak damping mode, as indicated by the modal analysis results, which reveals a damping ratio of 2.33% for the dominant oscillation mode of the power system.

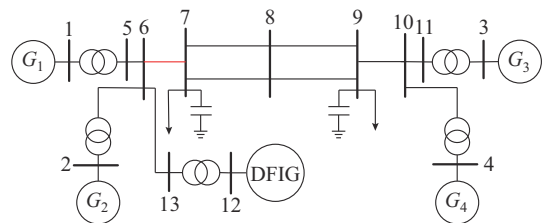


Fig. 4. Four-machine 11-bus power system with wind power sources.

The energy spectral function of the dissipation energy for each source in the power system is calculated using the measurement data. The dominant oscillation mode is then obtained using DESA. Analysis of the amplitude of the spectral function reveals that the dominant oscillation mode of the power system has a frequency of 0.6 Hz, as shown in Fig. 5, where $Load_1$ and $Load_2$ are two loads in the four-machine 11-bus power system.

Two peaks are observed near the frequency of 0.6 Hz, but they belong to the same mode. Therefore, the frequency corresponding to the maximum peak is used as the frequency for this mode. The phase of the spectral function is then analyzed to determine the phase value corresponding to a frequency of 0.6 Hz. The results indicate that G_1 , G_2 , and the new source belong to the same area, whereas G_3 and G_4 form another area.

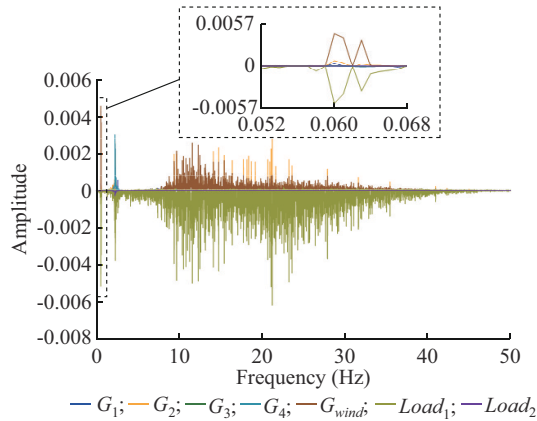


Fig. 5. Amplitude of spectral function of four-machine 11-bus power system.

A modal analysis is conducted with wind power source G_{wind} . Table I shows the comparison of modal analysis results.

TABLE I
COMPARISON OF MODAL ANALYSIS RESULTS OF FOUR-MACHINE 11-BUS POWER SYSTEM

Analysis method	Modal frequency (Hz)	Oscillation area division
Eigenvalue analysis	0.61	$(G_1, G_2), (G_3, G_4, G_{wind})$
DESA	0.60	$(G_1, G_2), (G_3, G_4, G_{wind})$

The modal analysis reveals that the dominant oscillation frequency is 0.61 Hz. The results for the oscillation area division are consistent with the results of DESA. This demonstrates the effectiveness of the DESA.

The damping ratio is currently considered as an assessment index. Given that damping is the sum of the contributions from the local damping of each generator and load in the power system, this paper validates the effectiveness of the local damping index GEDF by modifying the length of line L_{67} (red line in Fig. 4) and comparing the trends of the damping ratio and sum of GEDFs. The original length of L_{67} in the system is 10 km, and the length is increased or decreased in increments of 0.5 km to observe the trends in the GEDF indices. Figure 6 presents the results.

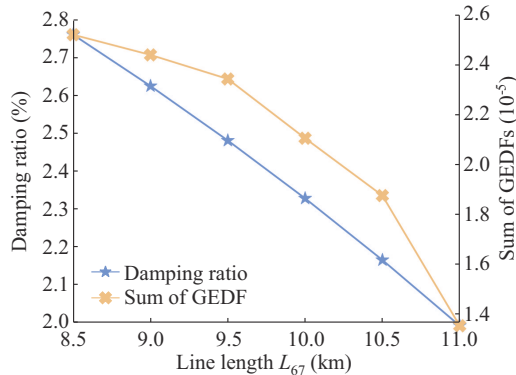


Fig. 6. Trends of damping ratio and sum of GEDFs of four-machine 11-bus power system.

The damping ratio of the power system is used to measure the stability of the corresponding modes. Figure 6 shows that as the line length increases from 8.5 km to 11

km, the damping ratio of the dominant oscillation mode monotonically decreases, which is in accordance with actual physical laws. Similarly, the sum of GEDFs decreases monotonically with the increase of line length, and the trend is consistent with that of the damping ratio. This preliminary analysis demonstrates the effectiveness of the GEDF indices.

Unlike traditional synchronous generators, traditional doubly-fed asynchronous wind turbines lack inertial response or primary frequency regulation capabilities due to the decoupling between their rotational speed and grid frequency, which affects the frequency regulation capabilities of power systems. Currently, virtual inertia control is integrated into wind turbine. However, the integration of virtual inertia control introduces coupling between the wind turbine and existing synchronous generators, causing significant changes in the electromechanical oscillation characteristics of the power system.

This paper analyzes and compares the presence of virtual inertia control in wind turbines as well as different droop control coefficient settings to demonstrate the effectiveness of the proposed method. Tables II-V present the results.

TABLE II
LOCAL DAMPING ASSESSMENT RESULT WITHOUT VIRTUAL INERTIA FOR WIND TURBINE

Generator or load	GEDF	Generator or load	GEDF
G_1	1.83×10^{-4}	G_{wind}	-1.97×10^{-5}
G_2	2.29×10^{-4}	$Load_1$	-1.45×10^{-4}
G_3	-8.04×10^{-5}	$Load_2$	-2.08×10^{-4}
G_4	-4.13×10^{-5}		

TABLE III
LOCAL DAMPING ASSESSMENT RESULT WITH A VIRTUAL INERTIA COEFFICIENT $K_{VD}=0.5$ FOR WIND TURBINE

Generator or load	GEDF	Generator or load	GEDF
G_1	2.01×10^{-5}	G_{wind}	1.41×10^{-4}
G_2	3.14×10^{-5}	$Load_1$	-1.74×10^{-4}
G_3	7.45×10^{-7}	$Load_2$	-1.68×10^{-5}
G_4	-8.70×10^{-7}		

TABLE IV
LOCAL DAMPING ASSESSMENT RESULT WITH A VIRTUAL INERTIA COEFFICIENT $K_{VD}=1$ FOR WIND TURBINE

Generator or load	GEDF	Generator or load	GEDF
G_1	5.21×10^{-6}	G_{wind}	1.89×10^{-4}
G_2	2.26×10^{-5}	$Load_1$	-1.89×10^{-4}
G_3	-4.76×10^{-7}	$Load_2$	-2.28×10^{-5}
G_4	-2.86×10^{-6}		

TABLE V
COMPARISON RESULTS OF SUM OF GEDFs AND DAMPING RATIO IN DIFFERENT SCENARIOS

Scenario	Sum of GEDFs	Damping ratio (%)
Without virtual inertia control	9.99×10^{-7}	1.28
With virtual inertia control ($K_{VD}=0.5$)	1.61×10^{-6}	2.25
With virtual inertia control ($K_{VD}=1$)	2.00×10^{-6}	2.33

The results show that the GEDF of the wind turbine is negative in the absence of virtual inertial control. Introducing virtual inertial control in a wind turbine changes the GEDF to a positive value, demonstrating that virtual inertial control tightens the coupling between the wind farm and the original power system, thereby substantially boosting the damping contribution of wind farm to the power system. In addition, an increase in the droop control coefficient K_{vD} amplifies the positive damping contribution from the wind turbine.

A comparison of the relationship between the sum of GEDFs and damping ratio of the power system across various scenarios clearly reveals that the integration of virtual inertia control into wind farms enhances the overall damping characteristics of the power system. In addition, the consistent trends in the changes of the sum of GEDFs and damping ratio underscore the effectiveness of the proposed method.

B. Actual Power System in Northwest China

An actual power system in Northwest China, as depicted in Fig. 7, is studied in this subsection. The power system includes wind power sources, photovoltaics (PVs), and high-voltage direct current components.

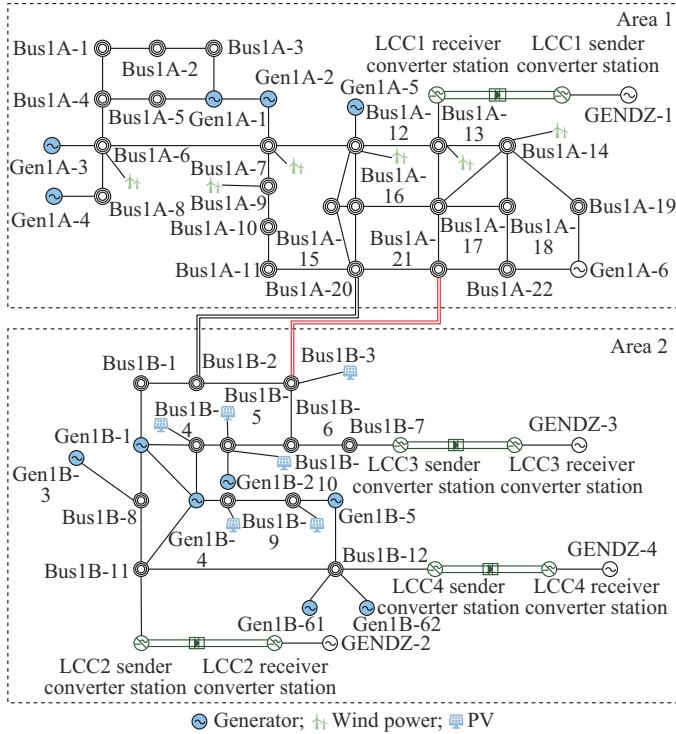


Fig. 7. Actual power system in Northwest China.

The DESA method is employed to extract the modal information of the power system. Figure 8 illustrates the amplitude of the energy spectral function, where G represents the generator, and the subscripts show the corresponding type (e.g., *wind* denotes the wind power generator represented by $A-F$; and PV denotes the PV generator represented by 1-6). The amplitude shows two peaks in the low-frequency interval corresponding to the frequencies of 1.51 Hz and 2.68 Hz. Given that the frequency interval for low-frequency oscillations should be between 0.2 Hz and 2.5 Hz, the domi-

nant oscillation mode frequency of the system is determined to be 1.51 Hz.

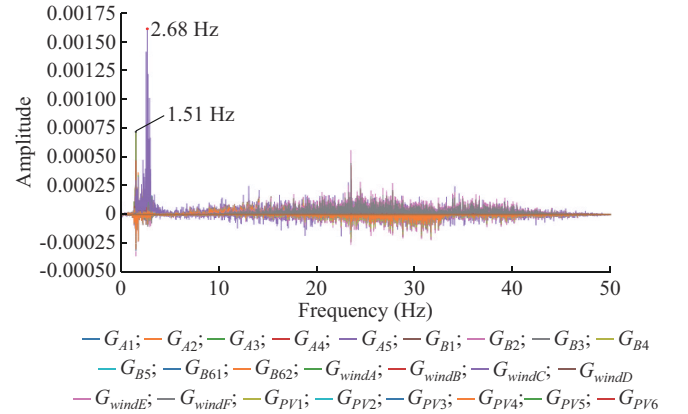


Fig. 8. Amplitude of energy spectrum function of actual power system.

The phase of each source at 1.51 Hz following the analysis of energy phase spectrum is obtained, as shown in Fig. 9. The sources in Areas 1 and 2 exhibit negative and positive phases, respectively. The phases of the wind and PV sources are zero. The oscillation areas of the power system show that the wind and PV sources do not participate in the oscillation.

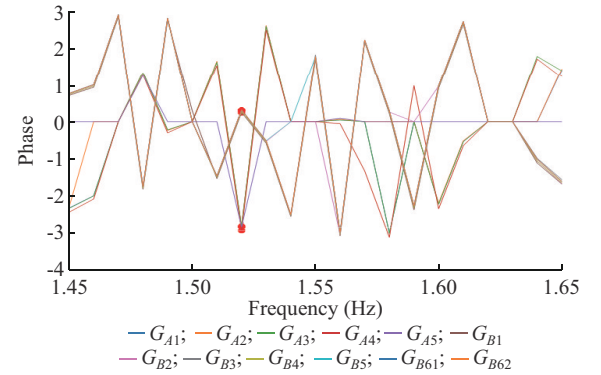


Fig. 9. Phase of energy spectrum function of actual power system.

Tables VI-IX present the results of the local damping assessment for the actual power system.

TABLE VI
GEDF VALUES FOR SYNCHRONOUS GENERATORS IN AREA 1

Generator	GEDF	Generator	GEDF
G_{A1}	2.65×10^{-5}	G_{A4}	1.72×10^{-5}
G_{A2}	2.65×10^{-5}	G_{A5}	1.26×10^{-5}
G_{A3}	2.65×10^{-5}		

TABLE VII
GEDF VALUES FOR WIND TURBINES IN AREA 1

Generator	GEDF	Generator	GEDF
G_{windA}	9.53×10^{-7}	G_{windD}	9.05×10^{-7}
G_{windB}	9.54×10^{-7}	G_{windE}	9.83×10^{-7}
G_{windC}	9.06×10^{-7}	G_{windF}	9.52×10^{-7}

TABLE VIII
GEDF VALUES FOR SYNCHRONOUS GENERATORS IN AREA 2

Generator	GEDF	Generator	GEDF
G_{B1}	-8.73×10^{-6}	G_{B5}	-1.32×10^{-5}
G_{B2}	-1.41×10^{-5}	G_{B61}	-1.29×10^{-5}
G_{B3}	-1.18×10^{-5}	G_{B62}	-1.29×10^{-5}
G_{B4}	-1.17×10^{-5}		

TABLE IX
GEDF VALUES FOR PV GENERATORS IN AREA 2

Generator	GEDF	Generator	GEDF
G_{PV1}	1.19×10^{-9}	G_{PV4}	9.48×10^{-10}
G_{PV2}	1.19×10^{-9}	G_{PV5}	8.81×10^{-10}
G_{PV3}	1.16×10^{-9}	G_{PV6}	1.57×10^{-9}

The effectiveness of the proposed method in the actual power system is also validated. The lengths of certain transmission lines in the power system are adjusted, and the trends of the system damping ratio and sum of GEDFs are compared, as shown in Fig. 10. The lengths of transmission lines AC_{13} and AC_{14} are modified (red lines in Fig. 7) to simulate the effect. The initial lengths of both lines are 512 km, and adjustments are made with 10 km intervals by either increasing or decreasing their lengths.

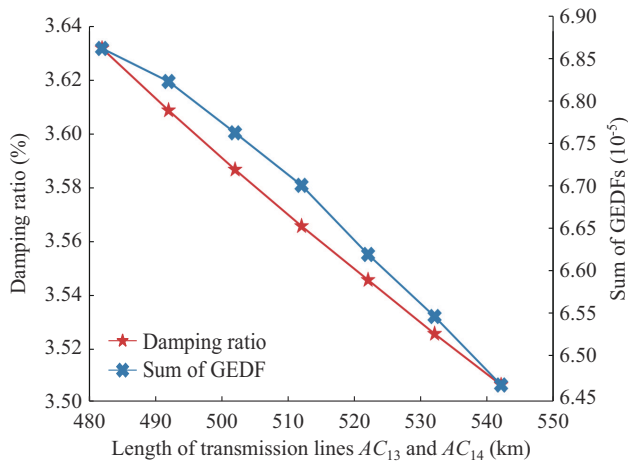


Fig. 10. Trends of damping ratio and sum of GEDFs of actual power system.

The results indicate that the damping ratio and sum of GEDFs decrease gradually with the increase of line length. The consistent trends in their variations confirm the effectiveness of the proposed method.

Load fluctuations with different signal-to-noise ratios (SNRs) are introduced into the power system to illustrate the stability of the proposed method. The relative magnitudes of the GEDF indices for various generators under different noise levels and the nature of their contributions to damping are analyzed. SNRs of 34, 35, and 36 are considered. Figures 11 and 12 present the simulation results.

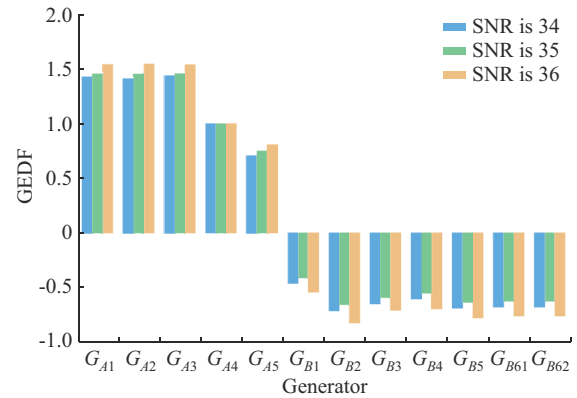
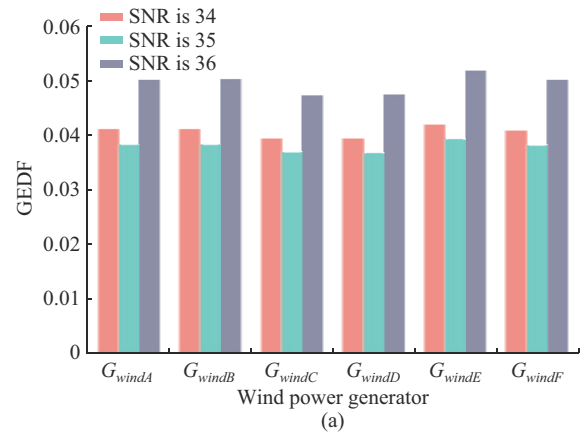
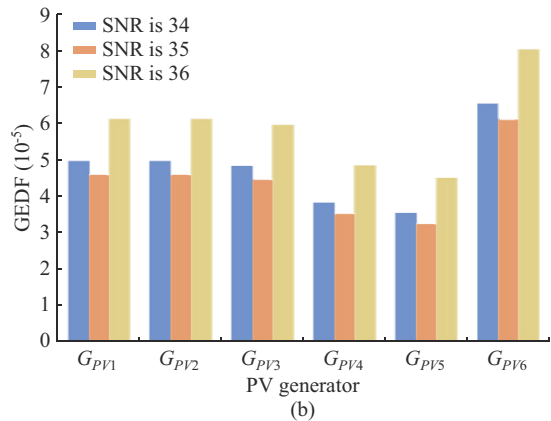


Fig. 11. GEDFs of synchronous generators under different SNRs.



(a)



(b)

Fig. 12. GEDFs of renewable energy generators under different SNRs. (a) Wind power generator. (b) PV generator.

The simulation results indicate that under different SNRs, the relative magnitudes of GEDFs of various generators in the power system and the nature of their damping contributions remain consistent. The results suggest the stability of the proposed method in conducting online tracking of local damping of individual generators. The renewable energy generators in the power system contribute minimally to the overall damping, whereas the synchronous generators play a major role.

To further demonstrate the effectiveness of the proposed method in power systems with renewable energy sources, this paper compares the local damping assessment results without wide-area damping controllers (WADCs) with those

with WADCs.

In the scenarios with WADCs, a compact design based on a power system stabilizer (PSS) is used, which adjusts the relative residual index by targeting specific dominant oscillation modes and by enhancing the control loop selection strategy. The PSS-based WADC is as straightforward as the classical PSS in which only two lead-lag phase compensation sources are incorporated [27].

The local damping indices of the power system with and without WADCs are assessed separately. The changes in the sum of GEDFs and damping ratio in both scenarios are compared, as presented in Table X.

TABLE X
COMPARISON OF MODAL ANALYSIS RESULTS OF ACTUAL POWER SYSTEM

Scenario	Sum of GEDFs	Damping ratio (%)
Without WADC	6.13×10^{-5}	3.57
With WADC	2.09×10^{-4}	4.01

Theoretically, the addition of a WADC to the power system should enhance its stability, which is confirmed by simulation results. The results also indicate that the damping ratio with WADC is higher than that without WADC. In addition, the sum of GEDFs is greater in the system with WADC than that without it. These findings are aligned with those of theoretical analysis and further validate the effectiveness of the proposed method.

VI. CONCLUSION

This paper proposes an online tracking method of local damping in power systems with high proportion of renewable energy sources under ambient data. The expression of dissipation energy in frequency domain at the generator ports is derived, which enables the spectral functions for the dissipation energy in each generator to be obtained. The dominant oscillation modes of the power system are identified by analyzing the amplitude and phase spectra of the spectral functions. The EDFs for each generator are then obtained by integration with the selected frequency interval. The simulation results demonstrate the effectiveness of the proposed method. The relationship between the eigenvalues and spectral functions is also analyzed. The indicators remain stable under varying ambient disturbances and accurately reflect the relationship between the damping contributions of different generators and their relative magnitudes. Notably, the proposed method requires the system to be in a normal operation state, and small disturbances may render the operation data unsuitable for the online tracking of local damping.

Future research work should consider the introduction of a decision-making step during the data acquisition process to extend the proposed method to a broad range of scenarios for the online tracking of local damping in power systems.

REFERENCES

- [1] T. Wang, M. Jin, Y. Li *et al.*, "Adaptive damping control scheme for wind grid-connected power systems with virtual inertia control," *IEEE Transactions on Power Systems*, vol. 37, no. 5, pp. 3902-3912, Sept. 2022.
- [2] S. Bu, W. Du, and H. Wang, "Investigation on probabilistic small-signal stability of power systems as affected by offshore wind generation," *IEEE Transactions on Power Systems*, vol. 30, no. 5, pp. 2479-2486, Sept. 2015.
- [3] S. Bu, W. Du, H. Wang *et al.*, "Probabilistic analysis of small-signal stability of large-scale power systems as affected by penetration of wind generation," *IEEE Transactions on Power Systems*, vol. 27, no. 2, pp. 762-770, May 2012.
- [4] B. Wang, D. Yang, and G. Cai, "Review of research on power system inertia related issues in the context of high penetration of renewable power generation," *Power System Technology*, vol. 44, no. 8, pp. 2998-3007, Aug. 2020.
- [5] Q. Wu, Y. Huang, Y. Zhou *et al.*, "Damping characteristics of synchronous motor-generator pair system for integration of new energy," *Automation of Electric Power Systems*, vol. 43, no. 15, pp. 80-86, Aug. 2019.
- [6] L. Chen, Y. Min, Y. Chen *et al.*, "Relationship between oscillation energy analysis and eigenvalue analysis and assessment of generator damping," *Automation of Electric Power Systems*, vol. 37, no. 19, pp. 33-40, Oct. 2013.
- [7] Z. Sun, Q. Jiang, J. Wang *et al.*, "Evaluation method of local damping of electromechanical oscillation of power systems containing wind turbines," *High Voltage Engineering*, vol. 47, no. 10, pp. 3452-3466, Oct. 2021.
- [8] L. Chen, Y. Chen, Y. Min *et al.*, "Low frequency oscillation analysis and oscillation source location based on oscillation energy, Part two: method for oscillation source location and case studies," *Automation of Electric Power Systems*, vol. 36, no. 4, pp. 1-5, Feb. 2012.
- [9] P. Kundur, "Small signal stability," in *Power System Stability and Control*. New York: McGraw-Hill, 1994.
- [10] S. Chou, X. Wang, and F. Blaabjerg, "Frequency-domain modal analysis for power-electronic-based power systems," *IEEE Transactions on Power Electronics*, vol. 36, no. 5, pp. 4910-4914, May 2021.
- [11] V. Aijarapu, "Reducibility and eigenvalue sensitivity for identifying critical generators in multimachine power systems," *IEEE Transactions on Power Systems*, vol. 5, no. 3, pp. 712-719, Aug. 1990.
- [12] M. Amin and M. Molinas, "Small-signal stability assessment of power electronics based power systems: a discussion of impedance- and eigenvalue-based methods," *IEEE Transactions on Industry Applications*, vol. 53, no. 5, pp. 5014-5030, Sept.-Oct. 2017.
- [13] H. Ghasemi and C. Canizares, "Damping torque estimation and oscillatory stability margin prediction," in *Proceedings of 2006 IEEE PES General Meeting*, Montreal, Canada, Jun. 2006, pp. 667-674.
- [14] Y. Yu and P. Li, "The impact of weak interconnection of bulk power grids to damping and dynamic stability of power systems," *Proceedings of CSEE*, vol. 25, no. 11, pp. 6-11, Jun. 2005.
- [15] G. Xu, J. Zhou, Z. Li *et al.*, "Damping torque coefficient affected by different rotor damping structures of turbo-generator during large disturbance," in *Proceedings of 2019 IEEE Energy Conversion Congress and Exposition (ECCE)*, Baltimore, USA, Oct. 2019, pp. 1729-1734.
- [16] Q. Dong, J. Sun, Q. Wu *et al.*, "A method for filtering low frequency disturbance in PMU data before coordinated usage in SCADA," *IEEE Transactions on Power Systems*, vol. 32, no. 4, pp. 2810-2816, Jul. 2017.
- [17] Z. Sun, J. Wang, C. Pan *et al.*, "Low-frequency oscillation area location method based on branch mode oscillation energy," *Proceedings of CSEE*, vol. 43, no. 17, pp. 6589-6601, Sept. 2023.
- [18] L. Chen, Y. Min, and W. Hu, "An energy-based method for location of power system oscillation source," *IEEE Transactions on Power Systems*, vol. 28, no. 2, pp. 828-836, May 2013.
- [19] L. Chen, Y. Min, and W. Hu, "Low frequency oscillation analysis and oscillation source location based on oscillation energy, Part one: mathematical foundation and energy flow computation," *Automation of Electric Power Systems*, vol. 36, no. 3, pp. 22-27, Feb. 2012.
- [20] Y. Hu, S. Bu, S. Yi *et al.*, "A novel energy flow analysis and its connection with modal analysis for investigating electromechanical oscillations in multi-machine power systems," *IEEE Transactions on Power Systems*, vol. 37, no. 2, pp. 1139-1150, Mar. 2022.
- [21] Y. Hu, S. Bu, X. Zhang *et al.*, "Connection between damping torque analysis and energy flow analysis in damping performance evaluation for electromechanical oscillations in power systems," *Journal of Modern Power Systems and Clean Energy*, vol. 10, no. 1, pp. 19-28, Jan. 2022.
- [22] Z. Sun, G. Cai, D. Yang *et al.*, "A method for the evaluation of generator damping during low-frequency oscillations," *IEEE Transactions on Power Systems*, vol. 34, no. 1, pp. 109-119, Jan. 2019.

- [23] L. Chen, Y. Chen, Y. Min *et al.*, "Low frequency oscillation analysis and oscillation source location based on oscillation energy, Part two: method for oscillation source location and case studies," *Automation of Electric Power Systems*, vol. 36, no. 4, pp. 1-5, Feb. 2012.
- [24] L. Chen, S. Ming, Y. Min *et al.*, "Online monitoring of generator damping using dissipation energy flow computed from ambient data," *IET Generation, Transmission & Distribution*, vol.11, no. 18, pp. 4430-4435, Dec. 2017.
- [25] L. Chen, Y. Min, Y. Chen *et al.*, "Evaluation of generator damping using dissipation energy dissipation and the connection with modal analysis," *IEEE Transactions on Power Systems*, vol. 29, no. 3, pp. 1393-1402, May 2014.
- [26] S. Maslennikov, B. Wang, and E. Litvinov, "Dissipating energy flow method for locating the source of sustained oscillations," *International Journal of Electrical Power & Energy Systems*, vol. 88, pp. 55-62, Jun. 2017.
- [27] J. Qi, Q. Wu, Y. Zhang *et al.*, "Unified residue method for design of compact wide-area damping controller based on power system stabilizer," *Journal of Modern Power Systems and Clean Energy*, vol. 8, no. 2, pp. 367-376, Mar. 2020.

Zhenglong Sun received the B.S., M.S., and Ph.D. degrees from Northeast Electric Power University, Jilin, China, in 2011, 2014, and 2018, respectively. He is currently a Lecturer of electrical engineering with Northeast Electric Power University. His research interests include stability analysis and control of renewable power system.

Zewei Li received the B.S. and M.S. degrees from Northeast Electric Power University, Jilin, China, in 2021 and 2024, respectively, where he is currently working toward the Ph. D. degree. His research interests include power system stability analysis and control.

Hao Yang received the B.S. degree from the Qilu University of Technology, Jinan, China, in 2011, the M.S. degree from North China Electric Power University, Beijing, China, in 2014, and the Ph.D. degree from Shandong University, Jinan, China, in 2019. He is currently an Associated Professor

with the School of Electrical Engineering, Northeast Electric Power University, Jilin, China. His research interests include stability and control in power system with renewable energy, and application of data-driven technique to power system.

Lixin Wang received the B.S., M.S., and Ph.D. degrees from Northeast Electric Power University, Jilin, China, in 2014, 2017, and 2021, respectively. She is currently a Teaching Assistant of electrical engineering with Northeast Electric Power University. Her research interests include power system stability analysis and control.

Bo Wang received the M.S. and Ph.D. degrees from Northeast Electric Power University, Jilin, China, in 2017 and 2020, respectively. He is currently a Lecturer of electrical engineering with Northeast Electric Power University. His research interests include power system dynamic stability mechanism, and data-based power system modeling and control.

Chao Pan received the B.S. degree from Beihua University, Jilin, China, in 2004, the M.S. degree from Northeast Electric Power University, Jilin, China, in 2007, and the Ph.D. degree from North China Electric Power University, Beijing, China, in 2013. His research interests include numerical calculation of electromagnetic fields and electromagnetic compatibility of power system.

Cheng Liu received the B.S. and M.S. degrees from Northeast Electric Power University, Jilin, China, in 2009 and 2012, respectively, and the Ph.D. degree from North China Electric Power University, Beijing, China, in 2017. He is currently a Lecturer of electrical engineering with Northeast Electric Power University. His research interests include renewable power system stability analysis and control.

Guowei Cai received the B.S. and M.S. degrees from Northeast Electric Power University, Jilin, China, in 1990 and 1993, respectively, and the Ph.D. degree from the Harbin Institute of Technology, Harbin, China, in 1999. He is currently a Professor of electrical engineering with Northeast Electric Power University. His research interests include power system stability analysis and control, and smart grid with renewable power generation.